

RESEARCH

Open Access



Ciprofol prevents ferroptosis in LPS induced acute lung injury by activating the Nrf2 signaling pathway

Qin Zhao^{1,2,3†}, Chang Kong^{1,2,3†}, Xiuyun Wu^{4†}, Yong Ling⁵, Jia Shi^{1,2,3}, Shaona Li⁴, Youzhuang Zhu⁴ and Jianbo Yu^{1,2,3,6*}

Abstract

Background Patients who suffered from sepsis-induced acute lung injury (ALI) always need sedation for mechanical ventilation in intensive care unit (ICU). Ciprofol (Cip), a novel intravenous anesthetic, was revealed to have anti-inflammatory and antioxidative properties. Ferroptosis, categorized as a type of newly non-apoptotic cell death, participates in the development of lung injury. This study aimed to identify the effect of ciprofol on sepsis-induced ALI and to determine whether ferroptosis is involved.

Methods and results To create ALI models, MLE12 alveolar epithelial cells and lipopolysaccharide (LPS)-stimulated C57BL/6J mice were used. Our results displayed that Cip reduced lung injury and ferroptosis. In the LPS-induced sepsis mice model, Cip pretreatment partially reduced respiratory system damage, as evaluated by HE, TUNEL and inflammatory factors. By raising GSH levels, ciprofol activated the Nrf2 antioxidative pathway, blocked ferroptosis, increased ferroptosis-related protein (GPX4 and SLC7A11) expressions, and reduced Fe²⁺ content, as well as MDA and 4-HNE levels. However, the protective effects of Cip on lung injury and ferroptosis diminished in Nrf2-KO mice. Additionally, Cip activated the Nrf2 pathway and reduced cell death by preventing detrimental lipid peroxidation and ferroptosis in vitro. However, these effects were not observed in siNrf2-treated cells.

Conclusion Our study demonstrated that Cip may prevent septic lung injury by suppressing ferroptosis through the Nrf2 pathway.

Keywords Ciprofol (Cip), Ferroptosis, Acute lung injury, Nuclear factor erythroid-2 related factor 2 (Nrf2), Glutathione peroxidase 4 (GPX4)

[†]Qin Zhao, Chang Kong and Xiuyun Wu have contributed equally to this work.

*Correspondence:

Jianbo Yu
30717008@nankai.edu.cn

¹Tianjin Nankai Hospital, Tianjin Medical University, Tianjin, China

²Tianjin Key Laboratory of Acute Abdomen Disease Associated Organ Injury and ITCWM Repair, Tianjin, China

³Institute of Integrative Medicine for Acute Abdominal Diseases, Tianjin, China

⁴Department of Anesthesiology, The Affiliated Hospital of Qingdao University, Qingdao, Shandong, China

⁵Department of Pharmacy, The Affiliated Hospital of Qingdao University, Qingdao, Shandong, China

⁶Department of Anesthesiology and Critical Care Medicine, Tianjin Nankai Hospital, Tianjin Medical University, Changjiang street, Nankai district, Tianjin 300000, China



Introduction

As a life-threatening organ dysfunction syndrome, sepsis is resulted from a uncontrolled response to the host's infection [1]. Recent progress in the pathobiology, epidemiology, and clinical trials of sepsis have indicated its higher morbidity and mortality in clinical practice [2]. During sepsis, the systemic inflammatory responses cause irreversible lung damage and finally develop into acute lung injury (ALI) which can subsequently deteriorate into acute respiratory distress syndrome (ARDS). ALI/ARDS which related to sepsis displays a higher mortality rate, compared to other causes [3]. The main symptoms of ARDS/ALI are an uncontrolled inflammatory response, alveolar epithelium injury, and destruction of endothelial barrier integrity, which causes inflammatory cell infiltration and diffuse alveolar and pulmonary interstitial edema [4, 5]. Therefore, the treatment of sepsis-induced ALI might depend on oxidative stress reduction in pulmonary epithelial cells and the maintenance of an intact alveolar epithelial barrier.

Classic clinical signs of ARDS/ALI include refractory hypoxemia and respiratory failure [6]. Mechanical ventilation is a common treatment for ARDS patients in Intensive Care Unit (ICU). Additionally, the patients undergoing mechanical ventilation usually require sedation and analgesia [7, 8]. At present, midazolam, dexmedetomidine and propofol are representative sedatives for sedation used in ICU patients. Midazolam is characterized by little effect on circulation, but it has the disadvantage of slow metabolism which may lead to accumulation and prolonged of mechanical ventilation [9]. Dexmedetomidine does not depress the respiratory and has both sedative and analgesic effects, but it also causes bradycardia and hypotension as side effects [10]. Compared with midazolam and dexmedetomidine, propofol offers a faster onset and recovery, which leads to faster wake up time and shorter hospital stay. However, propofol has a significant rate of hypotension due to systemic vasodilation, respiratory depression, as well as hypertriglyceridemia [11].

A 2,6-disubstituted phenol derivative, ciprofol is a newly developed intravenous anesthetic and is approved for induction and maintenance of general anesthesia, as well as intensive care sedation [12–14]. Ciprofol is about four to five times more potent than propofol and is more stable in circulation. In clinical trials, ciprofol shows similar tolerability and sedation characteristics compared to propofol for patients receiving mechanical ventilation in ICU [15, 16]. Recent studies have shown its significant anti-inflammatory and antioxidative activities. By regulating the Sirt1/Nrf2 pathway, ciprofol protects the heart from ISO-induced oxidative damage and inflammatory reaction [17].

Ferroptosis, a new type of regulated cell death, is manifested by iron -based lipid peroxidation and extensive generation of reactive oxygen species (ROS) in cells [18]. Moreover, ferroptosis is linked to several pathophysiological processes, including degenerative diseases, cancer, and ischemia-reperfusion injury [19–21]. A recent study showed that ferroptosis is crucial for sepsis-related organ injury. For example, ferroptosis inhibitor (Fer-1) can alleviate sepsis-related lung injury by inhibiting ferroptosis [22]. Additionally, melanin nanoparticles significantly alleviated myocardial injury by suppressing iron accumulation and attenuating oxidative stress in the LPS-induced murine sepsis model [23]. As an endogenous transcription factor, Nuclear factor erythroid 2-related factor 2 (NFE2L2/Nrf2) is closely associated with lipid peroxidation and iron metabolism. Nrf2 upregulation suppresses lipid peroxidation by modulating cystine/glutamate transporter (SLC7A11), glutathione (GSH), and glutathione peroxidase 4 (GPX4) in ferroptosis regulation [24, 25], and exerts a protective effect in lung injury.

A previous study showed that propofol can alleviate DOX-induced ferroptosis and protect cardiomyocytes from oxidative stress and inflammatory responses by activating Nrf2/GPX4 signaling in H9c2 cells [26]. Considering the similar chemical structure of ciprofol and propofol, whether ciprofol has a protective effect against organ damage through ferroptosis suppression remains unclear. Thus, our study aimed to investigate whether ciprofol conferred a strong anti-ferroptotic function in pulmonary epithelial cells after LPS stimulation. We also sought to explore the underlying mechanism of LPS-induced ALI.

Materials and methods

Animal model

Our animal experiments were approved by in advance the Animal Care and Use Committee of Tianjin Nankai Hospital (approval number No-NKYY-DWLL-2024-098) and conformed to the institutional guidelines for experimental animals. We used both 6 to 8-week-old healthy C57BL/6J male mice (Laboratory Animal Center of Tianjin Nankai Hospital) and Nrf2-knockout (Nrf2KO) male mice (Jiangsu Huachuang Sino Pharmaceutical Technology Co., Ltd) in our experiments. Animals under standard conditions had free access to diet and water, with a day–night cycle for 12 h at 25 °C. The mice were randomized to four groups ($n=6$ /group): control group, LPS group, LPS+Cip group, and Cip group, respectively. The LPS (Solarbio, Beijing, China) injection (10 mg/kg) via the tail vein was used to establish the sepsis-induced ALI model. According to a human-to-animal dose conversion guide [27] and its pharmacokinetic characteristics [12], the LPS+Cip group mice received intraperitoneal ciprofol (Haisco Pharmaceutical Group Co., Ltd., China)

instillation (50 mg/kg) for 2 h with reference to clinical dosages (0.5–2 mg/kg/h) of ciprofol before LPS stimulation. For ferroptosis detection, the mice were randomized to four groups ($n=6$ /group): control group, LPS group, LPS+ferrostatin-1(Fer) group, and LPS+Cip group. The mice in LPS+Fer-1 group were given an intraperitoneal injection with Fer-1 (Sigma, USA) (5 mg/kg) 2 h before LPS stimulation. In order to demonstrate the effect of the Nrf2 pathway in the Cip-mediated reduction in lung injury, mice were further divided into two groups ($n=6$ /group): LPS+Cip group and Nrf2 KO+LPS+Cip group, respectively. Following a 12-hour LPS treatment, mice were sacrificed, and their left lungs, blood, and bronchoalveolar lavage (BAL) fluid were taken for additional testing. To reduce the suffering of the mice, we used isoflurane (2–3%) to anesthetize them. After the mice were unconscious, they were sacrificed by cervical dislocation.

Histopathological analysis

After washing with PBS and fixing in 10% formalin fixation, we embedded the lung tissues in paraffin, and then cut tissues into 4- μ m slices on a microtome. Next, the hematoxylin and eosin (H&E) was used to stain the lung sections for histopathological analysis. A semiquantitative scoring system based on the following parameters was used to assess the level of lung injury: neutrophil infiltration, pulmonary edema, disorganization of lung parenchyma and hemorrhage. Briefly, the following rating scale was employed: 0=none, 1=light damage (25%), 2=moderate damage (50%), 3=severe damage (75%), and 4=extremely severe damage (approximately 100%) to score the degree of lesion in all samples. Two pathologists blinded to the experimental setup assessed the lung injury scores.

Cell culture and treatment

Mouse lung epithelial cell lines (MLE12) were cultured in the HITES medium in a 5% carbon dioxide humidified incubator at a temperature of 37 °C. The media was renewed every two to three days. When MLE12 cells reached 80–90% confluency, they were passaged to create a sepsis model. A range of LPS dosages (0, 0.1, 1, 5, 10, and 20 μ g/mL) were applied to MLE12 cells for 24 h. Additionally, Nrf2 siRNA (5'-AUUGAUGUUUCUGAUCUAUCACUTT-3'), obtained from Suzhou Gene Pharma Co. Ltd, was transfected into the cells.

Cell viability assay

A CCK-8 kit (Beyotime, Shanghai, China) was used for evaluating cell viability. MLE12 cells were inserted in a 96-well plate at a concentration of 3500 cells per well and cultured for 24 h. Subsequently, they were treated with LPS in different concentrations for 24 h. In some groups, ciprofol in different concentrations (0, 1.25, 2.5, 5, 10, and

20 μ M) was added before LPS insult for 2 h. Additionally, 10 μ L of CCK8 solution was directly added into each well, and the mixture was incubated at 37 °C for another 2.5 h. Intergroup cell viability was detected using a microplate reader at 450 nm.

Enzyme-linked immunosorbent assay (ELISA)

The BAL fluid supernatant of mice and cell cultures were collected and chemokine (TNF- α , IL-1 β , and IL-6) levels were determined with ELISA kits (F2132-B, F2040-B, F2163-B; Kexing, Shanghai, China), in accordance with the manufacturer's instructions. Subsequently, we measured optical density to determine the levels at 450 nm.

Mitochondrial membrane potential (MMP) assay

A JC-1 Mitochondrial membrane potential (MMP) Assay Kit (Jiancheng, Nanjing, China) was used to assess MMP changes. Following a 20-minute incubation period at 37 °C with the JC-1 solution, the cells were twice rinsed with incubation buffer. Further analyses were performed with a flow cytometer (NovoCyte543210110276, USA).

Malondialdehyde (MDA), superoxide dismutase (SOD), and glutathione (GSH) measurement

MDA, SOD, and GSH cellular concentrations were determined by their corresponding kits (A003-4-1, A001-3-2, A006-2-1; Jiancheng, Nanjing, China). Briefly, we rinsed lung tissues with PBS and homogenized them on ice. After centrifugation at 3500 \times g for 10 min, we collected the supernatant and incubated it with an assay solution. Using a microplate reader, the absorbance was determined at 450 nm. Furthermore, using a BCA protein assay kit (Beyotime, China), the MDA, SOD, and GSH levels were determined and standardized to protein levels.

Immunofluorescence assay

After three PBS washes, the samples were fixed for 30 min at room temperature using 4% paraformaldehyde. The cells were blocked using 4% rabbit serum for one hour at room temperature after being permeabilized for thirty minutes with 0.5% Triton X-100. After overnight incubation with primary antibody (1:150) at 4 °C, the cells were incubated for 1 h at 37 °C in the dark with secondary antibody (1:200). The samples were stained with DAPI, and a fluorescent microscope (panoramic scan, 3DHISTECH, Hungary) was used for observing protein expressions.

Western blot

Lung tissues and MLE12 cells were lysed in RIPA buffer (Beyotime, China) for 15 min on ice. The cell lysates were centrifuged at 12,000 rpm for 20 min at 4 °C to obtain cellular proteins. Then, the protein concentrations

were detected by a BCA protein assay kit (Thermo, USA). Protein samples in identical amounts from each group were subjected to 10% SDS-PAGE and then placed onto a PVDF membrane. Furthermore, the membranes were blocked with 5% skim milk in TBST at 37 °C for 1 h and incubated overnight with primary antibodies against Nrf2 (1:5000, Proteintech, 16396-1-AP), GPX4 (1:10000, Abcam, ab125066), 4-HNE (1:500, BIOSS, bs-6313R), PTGS2 (1:800, BOSTER, BM4419), SLC7A11 (1:500, Abcam, AB307601), and β -actin (1:2000, ZSGBBIO, TA-10) at 4 °C. The blots were incubated with a secondary antibody for one hour at room temperature following three TBST washes. Ultimately, the Bio-Rad enhanced chemiluminescence system was used to quantify the protein bands, and ImageJ was used to interpret the results.

Statistical analysis

Data were expressed as the mean \pm standard deviation ($S \pm D$). A t-test was applied to analyze the difference between the two groups. GraphPad Prism 9.2.0 was used for a one-way ANOVA followed by the Bonferroni post-test to compare multiple groups. All values of $p < 0.05$ were considered statistically significant.

Results

Ciprofol reduced LPS-induced ALI in mice

To confirm ciprofol's function in sepsis-induced ALI, we established an LPS-induced ALI model. The lung tissue's pathological changes were assessed via H&E and TUNEL staining as well as lung injury scores. Compared with the LPS group, LPS+Cip group reduced lung injury and inflammatory cell infiltration, destroyed pulmonary architecture, thickened the alveolar wall, and caused interstitial edema as well as alveolar hemorrhage (Fig. 1A). LPS+Cip group also showed a reduction in the dead cells' quantity (Fig. 1B and G). Additionally, the LPS+Cip group's lung injury score was lower than LPS group (Fig. 1C). Furthermore, ELISA results indicated that inflammatory cytokines IL-1 β , IL-6, TNF- α levels decreased by ciprofol addition (Fig. 1D-F). Thus, our results demonstrated that ciprofol could reduce sepsis-induced ALI and inflammatory responses in vivo.

Ciprofol prevented oxidative stress and ferroptosis in mice with LPS-induced ALI

MDA, GSH, and SOD levels were detected to determine the effects of oxidative stress, which initiated LPS-induced ALI. As seen in Fig. 2A-C, the MDA level was greater than that of the control group, as ciprofol administration reduced the MDA accumulation. Meanwhile, ciprofol restored the activities of GSH and SOD, which were significantly reduced with LPS treatment. Lipid peroxidation, Fe²⁺ accumulation, and mitochondrial morphological characteristics were detected to reveal

the ciprofol's preventive effect on ferroptosis. GPX4 upregulation effectively inhibits ferroptosis by modulating lipid peroxide accumulation. Compared with the control group, the GPX4 level significantly decreased while another ferroptosis marker, PTGS2 level, increased considerably in the LPS group's lung tissues. Meanwhile, ciprofol pretreatment increased and decreased GPX4 and PTGS2 levels, respectively (Fig. 2D, E and G). Additionally, ciprofol reduced the Fe²⁺ level of lung tissues compared with the LPS group (Fig. 2H). Western blot and immunohistochemical staining showed that the 4-hydroxy-2-nonenal (4-HNE) level decreased in the LPS+Cip group (Fig. 2D, F, I and K). Moreover, transmission electron microscopy (TEM) results indicated that mitochondria in the lung tissues of mice after LPS showed obvious alterations characteristic of ferroptosis, displaying decreased mitochondrial size, reduction of mitochondrial cristae, and impaired membrane integrity. This alteration improved following ciprofol treatment (Fig. 2J). We also further evaluated the effect of Fer-1 (a ferroptosis inhibitor) on LPS-induced ALI and achieved a similar effect as ciprofol treatment. Thus, these findings suggest that ciprofol might prevent sepsis-induced ALI by suppressing ferroptosis.

Ciprofol reduced LPS-induced MLE12 cell injury and inflammatory response

MLE12 cells were used to assess the ciprofol's preventive effects on LPS-induced ALI in vitro. LPS treatment reduced cell viability in a dose-dependent manner in MLE12 cells (Fig. 3A), and a dose of 10 μ g/mL was chosen for all subsequent experiments. As seen in Fig. 3B and C, ciprofol pretreatment increased cell viability in a dose-dependent manner while inhibiting LDH release. The flow cytometry results also showed that ciprofol pretreatment effectively promoted cell survival, compared with the LPS group (Fig. 3G and I). Additionally, IL-1 β , IL-6, and TNF- α levels were significantly higher in the LPS group than those in the control group; however, these effects were reversed by ciprofol addition (Fig. 3D-F). MMP is an important measure of mitochondrial function. We found that impaired MMP in LPS-treated MLE12 cells was reduced by ciprofol (Fig. 3H and J). Thus, we suggest that the ciprofol treatment could reduce LPS-induced MLE12 cell injury.

Ciprofol inhibited LPS-induced ferroptosis and reduced MLE12 cells' oxidative stress

To further confirm the ciprofol's effect on ferroptosis regulation, we used MLE12 cells. Ciprofol reduced MDA and intracellular ROS levels, while increased GSH and SOD levels were observed in the LPS group (Fig. 4A-D). Similar to the in vivo experiment, the ferroptosis level was determined by measuring Fe²⁺, GPX4, 4-HNE,

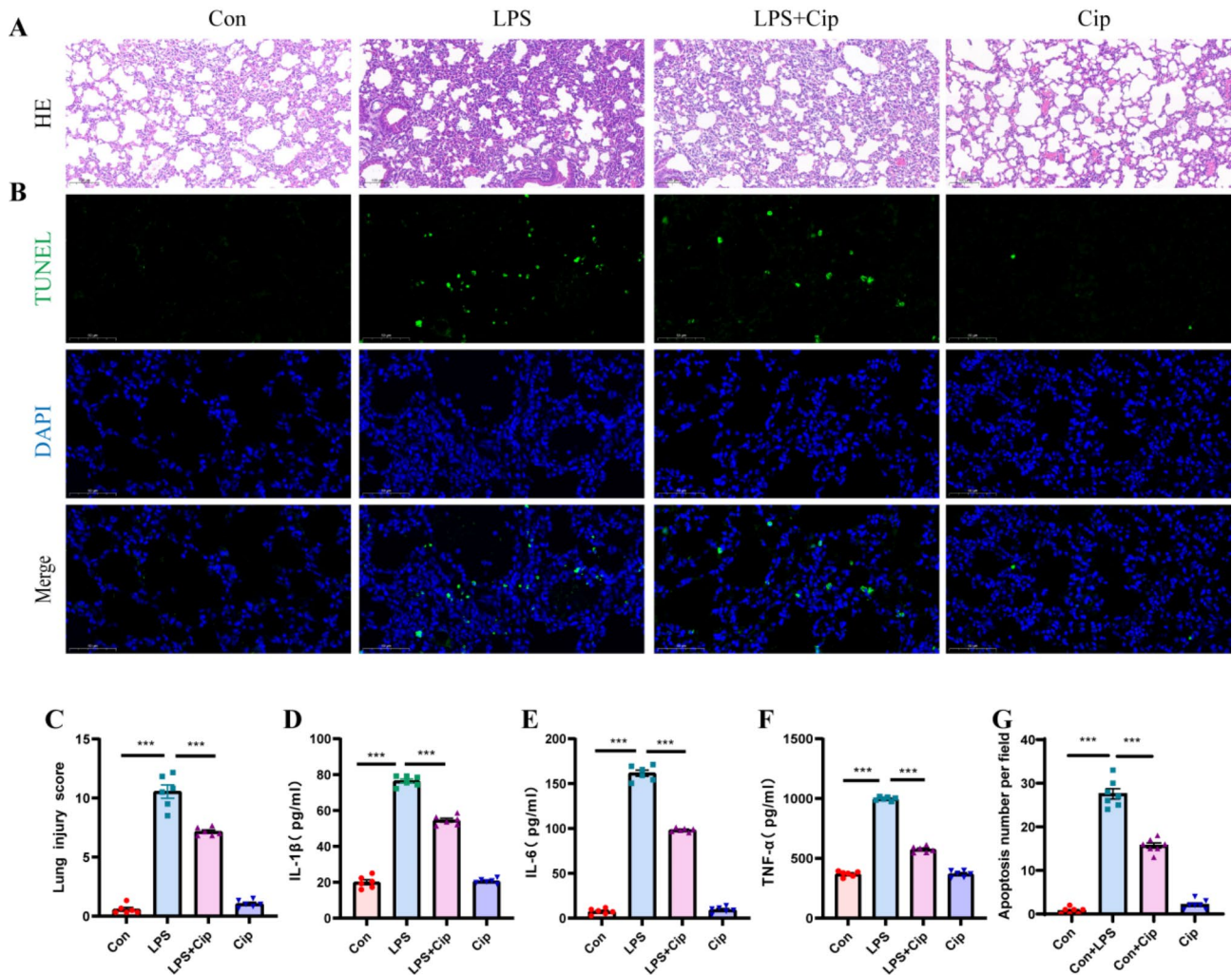


Fig. 1 Protective effects of ciprofol against LPS-induced ALI in mice. **A** Hematoxylin and eosin (HE) results showing the histopathological changes in the lung sections of ALI mice pretreated with or without ciprofol. Scale bar: 100 μm. **B** Representative images of terminal deoxynucleotidyl transferase dUTP nick end labeling (TUNEL) in lung tissue. Scale bar: 50 μm. **C** Lung injury score of lung tissues from each experimental group. **D-F** Proinflammatory cytokine IL-1β, IL-6, and TNF-α levels in murine lung tissues. **G** The number of TUNEL-positive cells was determined. Data are presented as Mean ± SD. (n = 6 per group). Statistical analysis was performed using one-way ANOVA. *p < 0.05, **p < 0.01, ***p < 0.001

and PTGS2 levels in the MLE12 cells. Western blot and immunofluorescence results indicated that GPX4 expression increased and 4-HNE expression decreased in the ciprofol or Fer-1 pretreatment group, compared with the LPS group (Fig. 4E-I and K). After detecting other ferroptotic phenotypes, the PTGS2 expression and Fe²⁺ accumulation increased after LPS administration, while both ciprofol and Fer-1 pretreatments decreased the PTGS2 expression and Fe²⁺ level (Fig. 4H, J). Thus, we confirmed the ciprofol's preventive effects on LPS-induced oxidative stress and ferroptosis inhibition.

Ciprofol upregulated Nrf2 expression to inhibit LPS-induced ferroptosis in MLE12 cells

To explore the ciprofol's preventive effects against LPS-induced ALI in MLE12 cells, we constructed the siRNA

against Nrf2. As seen in Fig. 5A and K, flow cytometry results indicated that the apoptosis rate in the Nrf2siRNA+LPS group was higher than in the LPS group. Furthermore, pretreatment with ciprofol reduced the LPS-induced apoptosis rate, whereas Nrf2 silencing attenuated these effects. Meanwhile, the CCK-8 assay revealed a similar result for cell viability and indicated that the ciprofol's preventive effects on LPS-induced cell injury were partially reversed by Nrf2 knockdown (Fig. 5B). In order to confirm the resistance of ciprofol to ferroptosis was dependent on Nrf2, we detected Fe²⁺, GPX4, 4-HNE, PTGS2, Nrf2, and SLC7A11 levels. Cell immunofluorescence and western blotting showed that Nrf2 expression was upregulated by ciprofol treatment, while Nrf2 protein level decreased after Nrf2 silencing (Fig. 5D, H, and J). Subsequently, the SLC7A11, as well

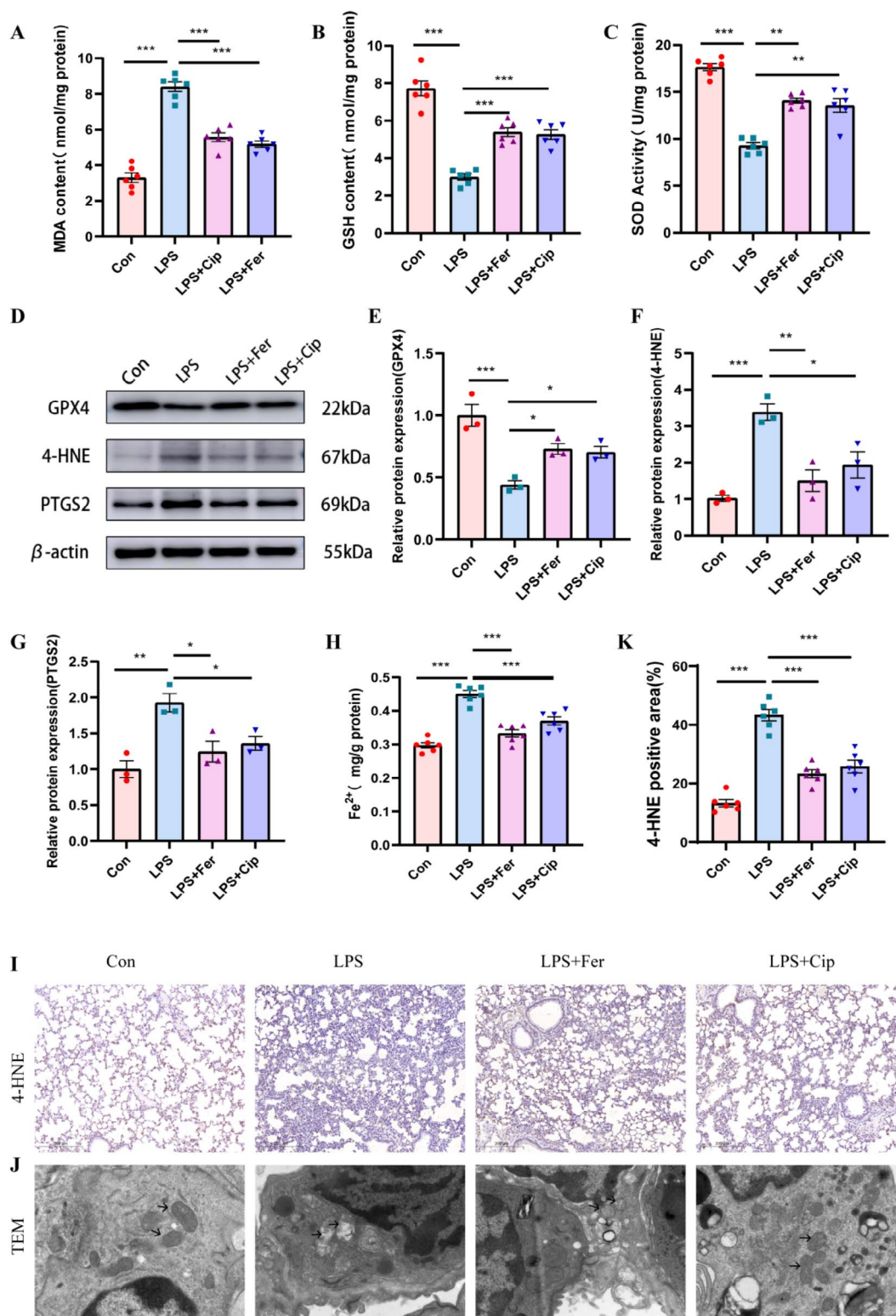


Fig. 2 ciprofol reduced LPS induced ferroptosis and increased antioxidant ability in mice. **A-C** Activities of malondialdehyde (MDA), glutathione (GSH), and superoxide dismutase (SOD) in the murine lung tissues ($n=6$ per group). **D-G** GPX4, 4-HNE and PTGS2 expressions in lung tissues detected by western blot ($n=3$ per group). **H** Expression level of Fe^{2+} in murine lung tissues ($n=6$ per group). **I** 4-HNE expressions in lung tissues detected by immunohistochemical staining. **J** Transmission electron microscopy images of representative mitochondrial structures (scale bar, 1.0 μ m). **K** Quantitative analysis of 4-HNE-positive area ($n=6$ per group). Data are presented as Mean \pm SD. Statistical analysis was performed using one-way ANOVA. * $p < 0.05$, ** $p < 0.01$, *** $p < 0.001$

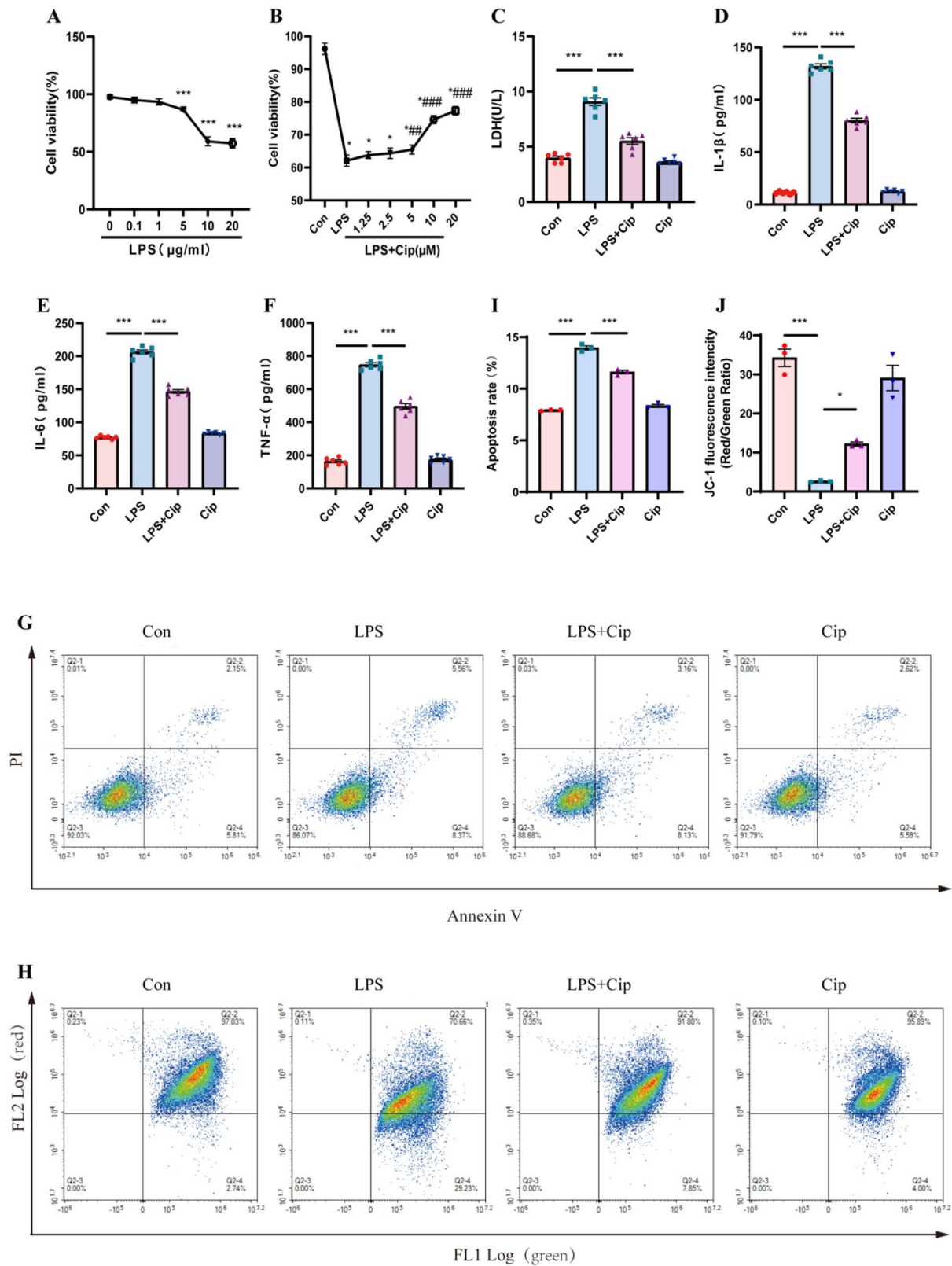


Fig. 3 (See legend on next page.)

(See figure on previous page.)

Fig. 3 Protective effects of ciprofol against LPS-induced MLE12 cell injury. **A** Cell viability was determined by CCK8 assays, after being treated with different concentrations of LPS for 24 h ($n=6$ per group). **B** Cell viability was determined by CCK8 assays, after ciprofol pretreatment with different concentrations prior to LPS treatment for 12 h ($n=6$ per group). **C** Lactate dehydrogenase (LDH) release in MLE12 cells ($n=6$ per group). **D-F** Proinflammatory cytokine IL-1 β , IL-6, and TNF- α levels in MLE12 cells ($n=6$ per group). **G** PI and Annexin V flow cytometry show apoptosis of MLE12 cells ($n=3$ per group). **H** Mitochondrial membrane potential (MMP) was determined by flow cytometry, after cells were stained with JC-1 indicated by the red/green fluorescence ratio ($n=3$ per group). **I** Apoptotic rate measured by Annexin V-FITC/PI flow cytometry ($n=3$ for each group). **J** Quantification of mitochondrial membrane potential after staining (Red/Green) ($n=3$ per group). Data are presented as Mean \pm SD. Statistical analysis was performed using one-way ANOVA. * $p < 0.05$, *** $p < 0.001$ vs. control; ## $p < 0.01$, ### $p < 0.001$ vs. LPS

as GPX4 levels decreased, and Fe²⁺ content, 4-HNE, as well as PTGS2 protein levels increased in the Nrf2siRNA+LPS group, compared with the LPS group. Thus, ciprofol pretreatment increased SLC7A11, and GPX4 levels and reduced Fe²⁺ content, 4-HNE, and PTGS2 levels; however, Nrf2 depletion majorly abolished its effect in MLE12 cells (Fig. 5D-I). Hence, this indicated that the ciprofol's ferroptosis resistance may be dependent on Nrf2 expression in vitro.

Ciprofol inhibited ferroptosis through Nrf2 activation in LPS-induced ALI mice

In order to further elucidate whether ciprofol's anti-ferroptotic function was Nrf2-dependent in vivo, we constructed the LPS-induced ALI models using Nrf2-knockout mice (Nrf2^{-/-}). Our results showed that Nrf2 deletion aggravated pathological changes in H&E-stained lung tissues (Fig. 6A). Subsequently, IL-1 β , IL-6, and TNF- α levels were higher in the Nrf2^{-/-} mice than in the ciprofol pretreated mice which indicated that ciprofol's preventive effect against inflammatory response was attenuated in Nrf2^{-/-} mice (Fig. 6B). The GSH and SOD levels increased while MDA level and Fe²⁺ content decreased after ciprofol treatment. However, the anti-ferroptosis effects were diminished in Nrf2^{-/-} mice (Fig. 6C). As shown in Fig. 6D-E, ciprofol was unable to conserve the decreased GPX4 and SLC7A11 levels, suggesting that Nrf2 deletion partially reversed the effects of ciprofol against ferroptosis. Thus, we determined that ciprofol prevented sepsis-induced ALI by inhibiting ferroptosis through a Nrf2-dependent mechanism.

Discussion

ALI is one of the critical diseases that has received increased public attention due to its high morbidity and mortality rates [28]. Sepsis remains one of the main causes of ALI [29], which causes alveolar-capillary barrier dysfunction. In sepsis-induced ALI, a burst of inflammatory cytokines and excessive ROS accumulation play a key role in the pathogenesis of lung injury [30]. Consequently, it is important to alleviate excessive inflammatory responses and ROS accumulation, thereby maintaining an intact alveolar epithelial barrier to combat ALI. Thus, we demonstrated that ciprofol could reduce sepsis-induced ALI by suppressing ferroptosis. Mechanistically, ciprofol treatment upregulated Nrf2

expression and promoted Nrf2-dependent target genes like GPX4 and SLC7A11. Hence, ciprofol might be a promising remedy for patients who need sedation and suffer from sepsis-induced ALI in ICUs.

A novel intravenous anesthetic, ciprofol, has a similar safety profile and chemical structure to propofol. Many studies have revealed propofol's protective effects on various lung diseases [31–33]. Compared with propofol, ciprofol has several advantages like rapid onset, faster recovery, a higher potency, reduced injection pain, and a lower mean arterial pressure (MAP) reduction [34, 35]. Additionally, ciprofol also protects the heart from ISO insults by suppressing oxidative stress and excessive inflammatory responses [17]. Another study indicated that ciprofol exhibited a protective effect against cerebral ischemia-reperfusion injury through attenuating lipid preoxidation and oxidative stress [36].

Thus, we designed a MLE12 cell impairment model, which was stimulated with LPS. Our results indicated that ciprofol refrained cell inflammation in vitro. Subsequently, we also found that severe lung injury occurred in mice in LPS-induced ALI, including varying degrees of edema, inflammatory cell infiltration, and lung tissue necrosis. Furthermore, the inflammatory factor (IL-1 β , IL-6, and TNF- α) levels were increased significantly in such mice. Ciprofol treatment **reduced** inflammation and **prevented** lung injury in vivo. These findings further solidified the fact that ciprofol **might prevent** sepsis-induced ALI by suppressing excessive inflammatory responses.

Different from other programmed cell deaths, ferroptosis is a novel Fe²⁺-dependent programmed cell death that is closely related to redox equilibrium and lipid metabolism. Several studies have showed that ferroptosis can induce the pathologic mechanism of sepsis-induced ALI [37–39]. Hence, ferroptosis inhibition might reduce tissue injury by using either ferroptosis inhibitors or Fe²⁺ chelation. We also verified that ferroptosis participated in the process of sepsis-induced lung injury. Ferroptosis indicators significantly increased, and mitochondrial shrinkage appeared after LPS treatment in both vivo and in vitro. Additionally, ciprofol exhibited an antioxidant effect and suppressed ROS production. Thus, we investigated the relationship between ciprofol and ferroptosis in our study. It was found that ciprofol treatment increased GSH and GPX4 levels, and reduced ROS production as

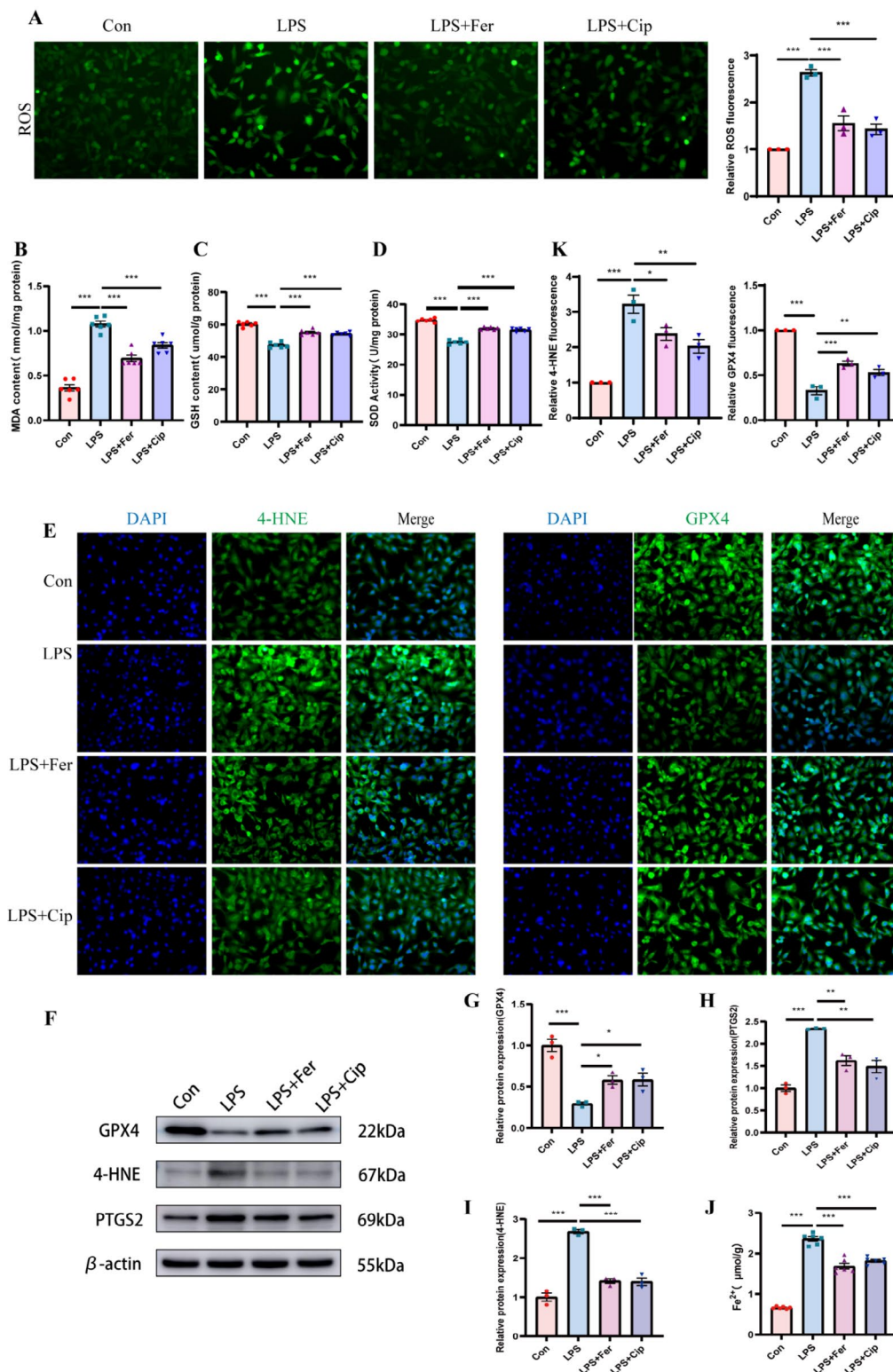


Fig. 4 ciprofol reduced LPS induced ferroptosis and increased antioxidant ability in MLE12 cells. **A** ROS production detected by immunofluorescence and its quantification analysis ($n=3$ for each group). **B-D** Activities of malondialdehyde (MDA), glutathione (GSH), and superoxide dismutase (SOD) in MLE12 cells ($n=6$ for each group). **E-K** Representative immunofluorescence images of 4-HNE, GPX4 and the quantification analysis in MLE12 cells ($n=3$ for each group). **F-I** GPX4, 4-HNE and PTGS2 expressions in MLE12 cells detected by western blot ($n=3$ for each group). **J** Expression level of Fe²⁺ in MLE12 cells ($n=6$ for each group). Data are presented as Mean \pm SD. Statistical analysis was performed using one-way ANOVA. * $p < 0.05$, ** $p < 0.01$, *** $p < 0.001$

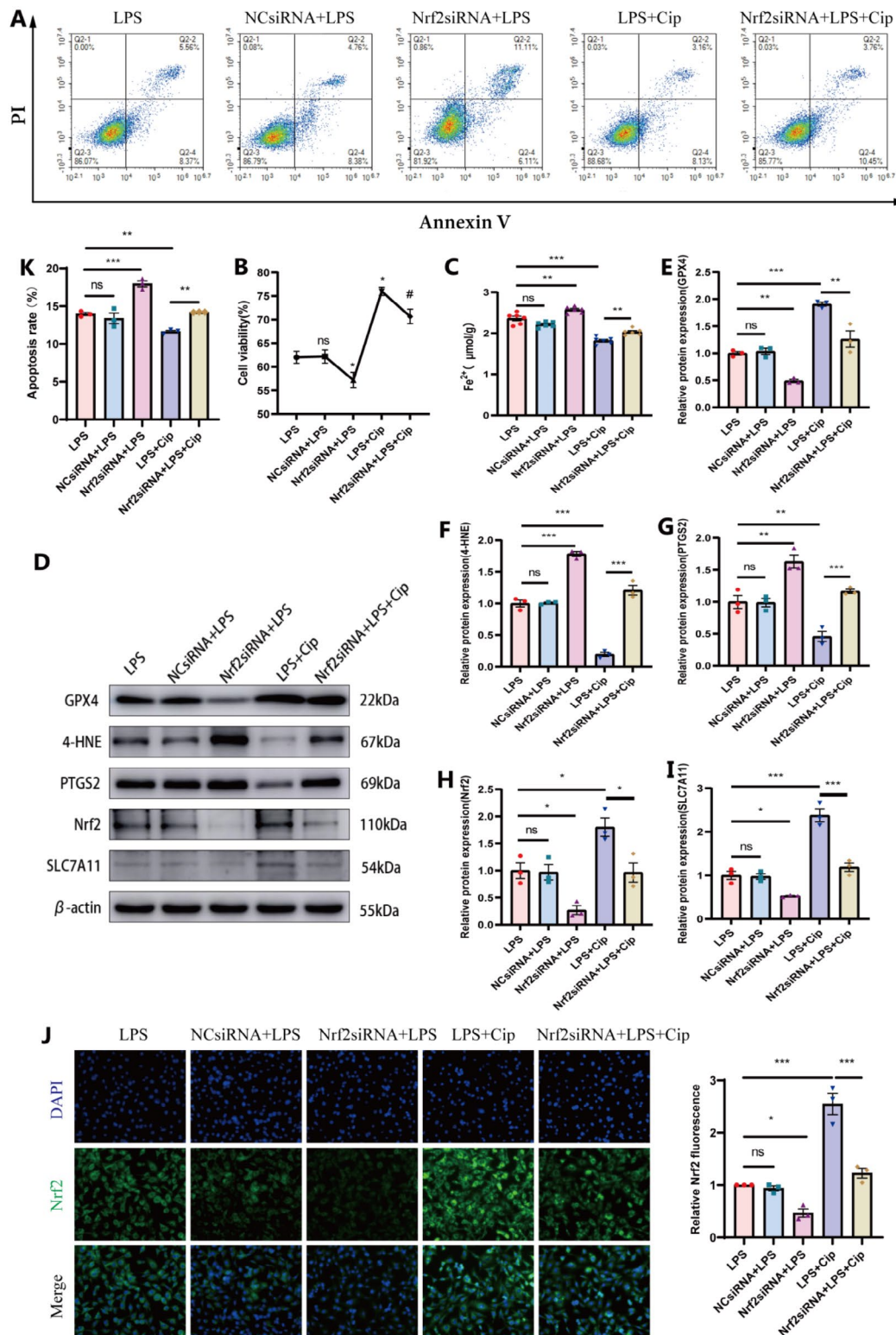


Fig. 5 ciprofol reduced LPS induced ferroptosis through Nrf2-dependent pathways in MLE12 cells. **A** Cell apoptosis detected by flow cytometry. **B** Cell viability determined by CCK8 assays ($n=6$ for each group). * $P < 0.05$ vs.LPS group; # $P < 0.05$ vs.LPS+ Cip group. **C** Expression level of Fe²⁺ in MLE12 cells. **D-I** GPX4, 4-HNE, PTGS2, Nrf2 and SL7A11 expressions in MLE12 cells detected by western blot ($n=3$ for each group). **J** Representative immunofluorescence images of Nrf2 and its quantification analysis in MLE12 cells ($n=3$ for each group). **K** Apoptotic rate measured by Annexin V-FITC/PI flow cytometry ($n=3$ for each group). Data are presented as Mean \pm SD. Statistical analysis was performed using one-way ANOVA.* $p < 0.05$, ** $p < 0.01$, *** $p < 0.001$

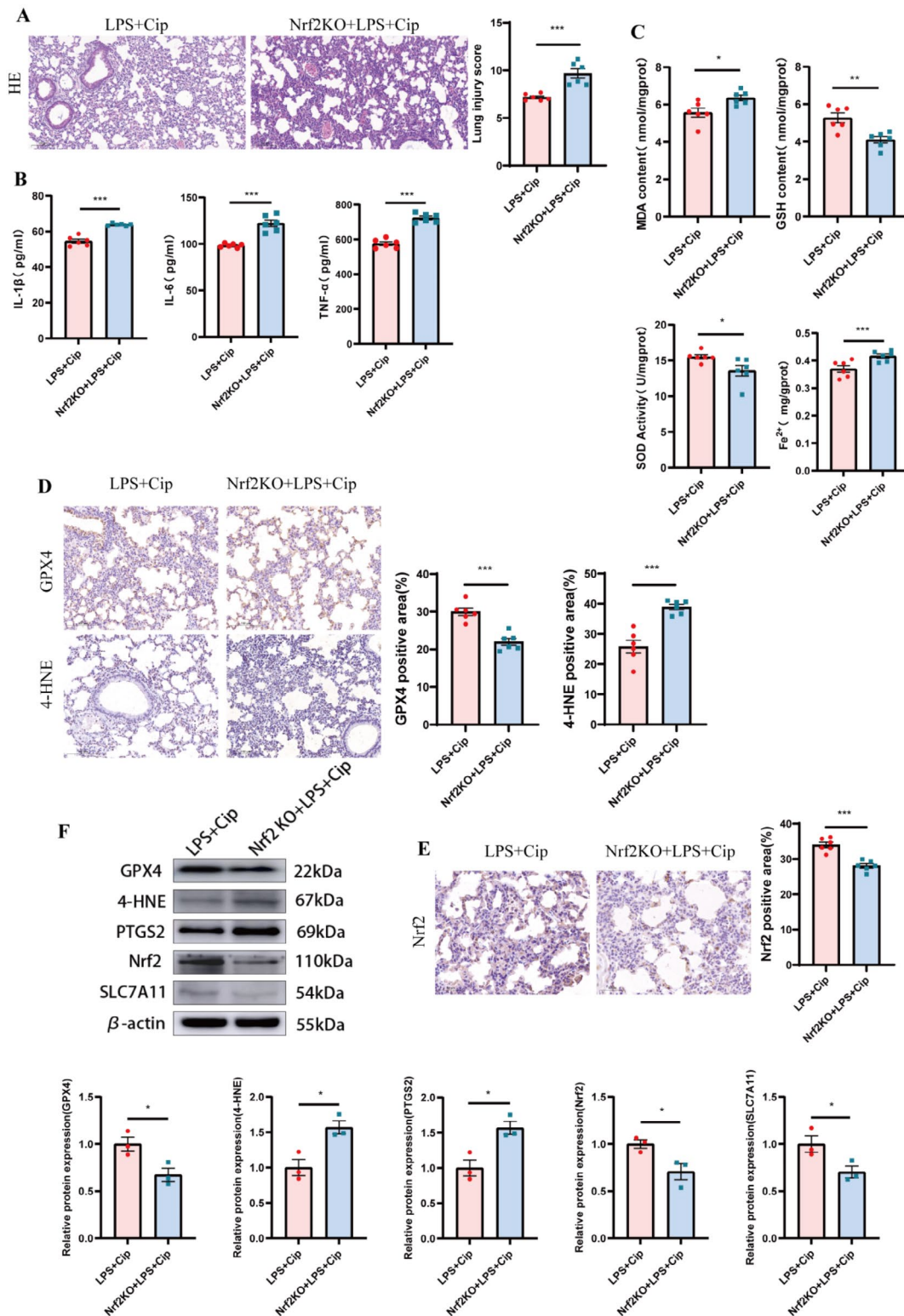


Fig. 6 The inhibition of ciprofol on ferroptosis was abolished in Nrf2 KO mice. **A** Representative HE staining images and lung injury score of the lung tissues ($n=6$ for each group). **B** Proinflammatory cytokine IL-1 β , IL-6, and TNF- α levels in lung tissues ($n=6$ for each group). **C** Activities of MDA, GSH, SOD and Fe $^{2+}$ content in lung tissues ($n=6$ for each group). **D** GPX4, 4-HNE expressions detected by immunohistochemical staining and the quantification analysis in lung tissues ($n=3$ for each group). **E** Nrf2 expressions detected by immunohistochemical staining and the quantification analysis in lung tissues ($n=3$ for each group). **F** GPX4, 4-HNE, PTGS2, Nrf2 and SL7A11 expressions detected by western blot in lung tissues ($n=3$ for each group). Data are presented as Mean \pm SD. Statistical analysis was performed using t-test. * $p < 0.05$, ** $p < 0.01$, *** $p < 0.001$

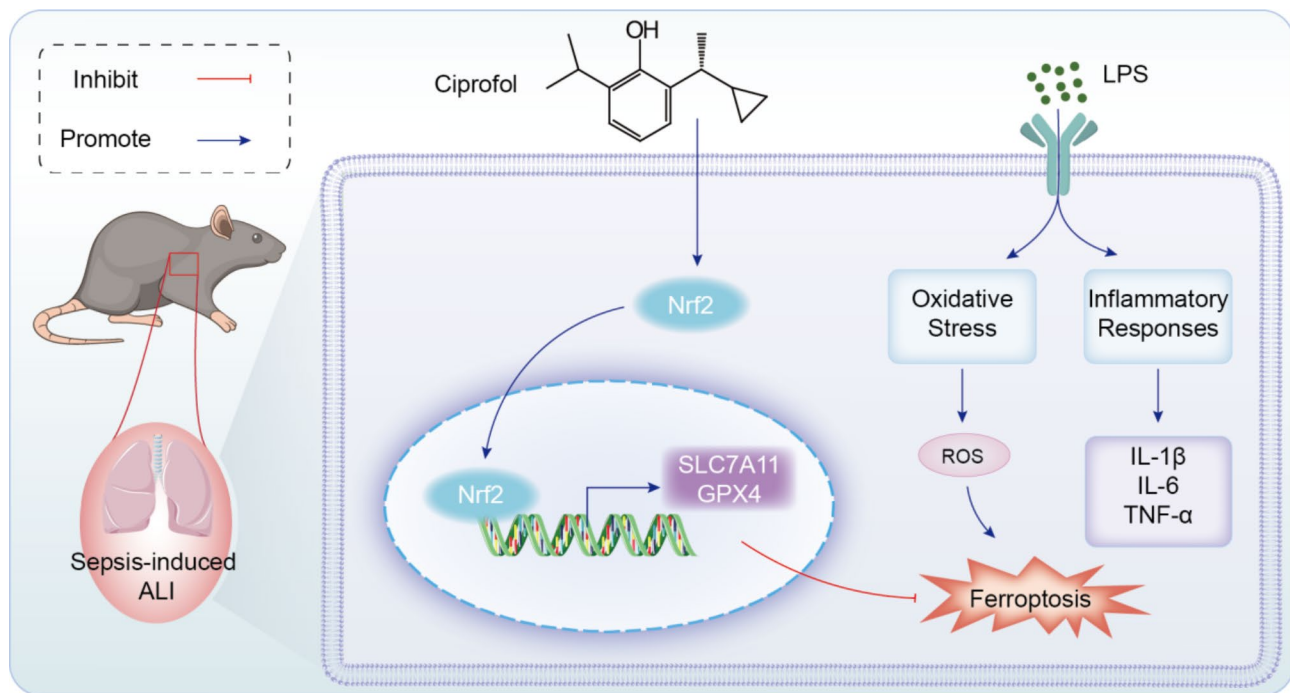


Fig. 7 Graphical abstract of ciprofol reduce sepsis-induced ALI. The possible pathways by which ciprofol antioxidative properties prevent ferroptosis in sepsis-induced ALI. Ciprofol upregulated Nrf2 expression and promoted the transcription of target genes, including SLC7A11 and GPX4. They helped to prevent ferroptosis induced by LPS and reduce sepsis-induced ALI

well as lipid peroxidation markers (MDA and 4HNE) in lung tissue and alveolar epithelial cells. Thus, our study is the first one to demonstrate that ciprofol may inhibit ferroptosis by activating the antioxidant system, thereby accounting for ciprofol's preventive effects in sepsis-induced ALI.

We further elucidated the potential ciprofol mechanisms that help in suppressing ferroptosis in sepsis-induced ALI. GPX4, a phospholipid hydroperoxidase, is a central regulator of ferroptosis [40] and uses GSH to eliminate membrane phospholipid hydroperoxides for ferroptosis suppression. As a major component of the glutamate/cystine antiporter system x_c^- , Slc7A11 regulates the downstream synthesis of GSH [41]. Additionally, the downstream target genes, GPX4 and SLC7A11 are transcriptionally regulated by Nrf2 [42, 43], and their reductions can be used as ferroptosis markers. We also found that ciprofol treatment upregulated Nrf2 and its downstream antioxidative genes, and reduced lipid peroxidation as well as ROS production. Additionally, Nrf2 deficiency in Nrf2^{-/-} mice and by siRNA in cells partially reversed ciprofol's preventive effects against LPS-induced ALI, thereby indicating that ciprofol might inhibit ferroptosis through Nrf2-dependent pathways (Fig. 7). Due to the multifaceted role of Nrf2 in regulating downstream genes, there may other pathways and other types of cell death which involved in the contribution of Nrf2 downstream of ciprofol treatment. In the future, we will also apply multi-omics technologies, such as sequencing and proteomics, to

detect the key molecules of Nrf2 downstream. Also, precise molecular processes should be further determined to better understand the direct target of ciprofol on the Nrf2 signaling pathway.

Our study had several limitations. In the current investigation, only alveolar epithelial cells were used, additional studies are needed to confirm the effect of ciprofol on other pulmonary inflammatory cells.

tightly connected with lung damage, such as lymphocytes and neutrophils. Moreover, follow-up studies are required to investigate the possibility that ciprofol regulates ferroptosis through other signaling pathways, such as the FSP1-CoQ10-NAD(P)H pathway and the ATG5-ATG7-NCOA4 pathway. In addition, we did not compare ciprofol with propofol in this experiment, which can better identify whether the anti-oxidant/anti-ferroptotic effect of ciprofol is solely related to this particular phenol derivative or is also observed in other derivatives such as propofol. Also, as an intravenous anesthetic, ciprofol was administered by intraperitoneal injection in this study, which was not consistent with clinical use to some extent.

In conclusion, we demonstrated that ciprofol could exerted preventive effects on sepsis-induced ALI. Mechanically, ciprofol reduced oxidative stress and inhibited ferroptosis in an Nrf2-dependent manner.

Abbreviations

Cip	Ciprofol
ALI	Acute lung injury

LPS	Lipopolysaccharide
HE	Hematoxylin and eosin
ELISA	Enzyme-linked immunosorbent assay
TUNEL	Terminal deoxynucleotidyl transferase (TdT) -mediated dUTP nick end labeling
Nrf2	Nuclear factor-2 associated factor 2
MDA	Malondialdehyde
GPX4	Glutathione Peroxidase 4
4-HNE	4-hydroxynonenal
PTGS2	Prostaglandin-endoperoxide synthase 2

Supplementary Information

The online version contains supplementary material available at <https://doi.org/10.1186/s12890-024-03415-w>.

Supplementary Material 1
Supplementary Material 2
Supplementary Material 3
Supplementary Material 4

Acknowledgements

This research was supported by the Youth Science Foundation of Affiliated Hospital of Qingdao University (No.QDFYQN2023230). The authors also thank the Laboratory Animal Research Center and the Institute of Acute Abdominal Diseases of Integrated Traditional Chinese and Western Medicine in Tianjin Nankai Hospital for technical assistance.

Author contributions

Q. Z., C. K., X. Y. W. designed the whole research, analyzed all results, and wrote the manuscript; J. B. Y. provided technical and material support; Y. L., J. S. participated in most of the experiments; Q. Z., C. K. performed development of methodology and writing, review and revision of the paper; S. N. L. and Y. Z. Z. helped in performing experiments; Q. Z. critically reviewed the manuscript. All the authors did final approval of the version to be submitted.

Funding

Our research was backed by the Youth Science Foundation of Affiliated Hospital of Qingdao University (No.QDFYQN2023230).

Data availability

The data supporting the conclusions of this article will be made available by the corresponding author without undue reservation. 30717008@nankai.edu.cn.

Declarations

Ethics approval and consent to participate

All animal experiments were conducted in accordance with Tianjin Medical Experimental Animal Care standards, and animal operations were approved by the Animal Care and Use Committee of Tianjin Nankai Hospital (Approval NO. No-NKYY-DWLL-2024-098). The study was reported in accordance with ARRIVE guideline.

Consent for publication

Not applicable.

Clinical trial number

Not applicable.

Competing interests

The authors declare no competing interests.

Received: 6 June 2024 / Accepted: 25 November 2024

Published online: 28 November 2024

References

- Singer M, Deutschman CS, Seymour CW, Shankar-Hari M, Annane D, Bauer M, Bellomo R, Bernard GR, Chiche JD, Cooper-Smith CM, Hotchkiss RS, Levy MM, Marshall JC, Martin GS, Opal SM, Rubenfeld GD, van der Poll T, Vincent JL, Angus DC. The Third International Consensus definitions for Sepsis and septic shock (Sepsis-3). *JAMA*. 2016;315(8):801–10. <https://doi.org/10.1001/jama.2016.0287>.
- Rudd KE, Johnson SC, Agesa KM, Shackelford KA, Tsoi D, Kievlan DR, Colombara DV, Ikuta KS, Kisssoon N, Finfer S, Fleischmann-Struzek C, Machado FR, Reinhart KK, Rowan K, Seymour CW, Watson RS, West TE, Marinho F, Hay SI, Lozano R, Lopez AD, Angus DC, Murray CJL, Naghavi M. Global, regional, and national sepsis incidence and mortality, 1990–2017: analysis for the global burden of Disease Study. *Lancet*. 2020;395(10219):200–11. [https://doi.org/10.1016/S0140-6736\(19\)32989-7](https://doi.org/10.1016/S0140-6736(19)32989-7).
- Englert JA, Bobba C, Baron RM. Integrating molecular pathogenesis and clinical translation in sepsis-induced acute respiratory distress syndrome. *JCI Insight*. 2019;4(2):e124061. <https://doi.org/10.1172/jci.insight.124061>.
- Bellani G, Laffey JG, Pham T, Fan E, Brochard L, Esteban A, Gattinoni L, van Haren F, Larsson A, McAuley DF, Ranieri M, Rubenfeld G, Thompson BT, Wrigg H, Slutsky AS, Pesenti A, LUNG, SAFE Investigators; ESICM Trials Group. Epidemiology, patterns of Care, and mortality for patients with Acute Respiratory Distress Syndrome in Intensive Care Units in 50 countries. *JAMA*. 2016;315(8):788–800. <https://doi.org/10.1001/jama.2016.0291>.
- Bos LDJ, Ware LB. Acute respiratory distress syndrome: causes, pathophysiology, and phenotypes. *Lancet*. 2022;400(10358):1145–56. [https://doi.org/10.1016/S0140-6736\(22\)01485-4](https://doi.org/10.1016/S0140-6736(22)01485-4).
- Saguil A, Fargo MV. Acute respiratory distress syndrome: diagnosis and management. *Am Fam Physician*. 2020;101(12):730–8.
- Chanques G, Constantin JM, Devlin JW, Ely EW, Fraser GL, Gélinas C, Girard TD, Guérin C, Jabaudon M, Jaber S, Mehta S, Langer T, Murray MJ, Pandharipande P, Patel B, Payen JF, Puntillo K, Rochweg B, Shehabi Y, Strøm T, Olsen HT, Kress JP. Analgesia and sedation in patients with ARDS. *Intensive Care Med*. 2020;46(12):2342–56. <https://doi.org/10.1007/s00134-020-06307-9>.
- Pearson SD, Patel BK. Evolving targets for sedation during mechanical ventilation. *Curr Opin Crit Care*. 2020;26(1):47–52. <https://doi.org/10.1097/MCC.0000000000000687>.
- Zhou Y, Yang J, Wang B, Wang P, Wang Z, Yang Y, Liang G, Jing X, Jin X, Zhang Z, Deng Y, Hu C, Liao X, Yin W, Tang Z, Tian Y, Tao L, Kang Y. Sequential use of midazolam and dexmedetomidine for long-term sedation may reduce weaning time in selected critically ill, mechanically ventilated patients: a randomized controlled study. *Crit Care*. 2022;26(1):122. <https://doi.org/10.1186/s13054-022-03967-5>.
- Lewis K, Alshamsi F, Carayannopoulos KL, Granholm A, Pitararu J, Al Duhaib Z, Chaudhuri D, Spatafora L, Yuan Y, Centofanti J, Spence J, Rochweg B, Perri D, Needham DM, Holbrook A, Devlin JW, Nishida O, Honarmand K, Ergon B, Khorochkov E, Pandharipande P, Alshahrani M, Karachi T, Soth M, Shehabi Y, Møller MH, Alhazzani W. GUIDe group. Dexmedetomidine vs other sedatives in critically ill mechanically ventilated adults: a systematic review and meta-analysis of randomized trials. *Intensive Care Med*. 2022;48(7):811–40. <https://doi.org/10.1007/s00134-022-06712-2>.
- Buckley MS, Agarwal SK, MacLaren R, Kane-Gill SL. Adverse hemodynamic events Associated with Concomitant Dexmedetomidine and Propofol for Sedation in mechanically ventilated ICU patients. *J Intensive Care Med*. 2020;35(12):1536–45. <https://doi.org/10.1177/0885066619884548>.
- Liao J, Li M, Huang C, Yu Y, Chen Y, Gan J, Xiao J, Xiang G, Ding X, Jiang R, Li P, Yang M. Pharmacodynamics and Pharmacokinetics of HSK3486, a novel 2,6-Disubstituted Phenol Derivative as a General Anesthetic. *Front Pharmacol*. 2022;13:830791. <https://doi.org/10.3389/fphar.2022.830791>.
- Zhong J, Zhang J, Fan Y, Zhu M, Zhao X, Zuo Z, Zhou X, Miao C. Efficacy and safety of Ciprofol for procedural sedation and anesthesia in non-operating room settings. *J Clin Anesth*. 2023;85:111047. <https://doi.org/10.1016/j.jclinan.2022.111047>.
- Liu Y, Peng Z, Liu S, Yu X, Zhu D, Zhang L, Wen J, An Y, Zhan L, Wang X, Kang Y, Pan A, Yan J, Zhang L, Liu F, Zeng J, Lin Q, Sun R, Yu J, Wang H, Yao L, Chen C, Liu N, Nie Y, Lyu J, Wu K, Wu J, Liu X, Guan X. Efficacy and safety of Ciprofol Sedation in ICU patients undergoing mechanical ventilation: a Multicenter, Single-Blind, randomized, Noninferiority Trial. *Crit Care Med*. 2023;51(10):1318–27. <https://doi.org/10.1097/CCM.0000000000005920>.
- Akhtar SMM, Fareed A, Ali M, Khan MS, Ali A, Mumtaz M, Kirchoff R, Asghar MS. Efficacy and safety of Ciprofol compared with propofol during general anesthesia induction: a systematic review and meta-analysis of randomized

- controlled trials (RCT). *J Clin Anesth.* 2024;94:111425. <https://doi.org/10.1016/j.jclinane.2024.111425>.
16. Liu L, Wang K, Sun Z, Yan P, Hu M, Liu X, Chen M, Wu N, Xiang X. Pharmacokinetics and exposure-safety relationship of ciprofol for sedation in mechanically ventilated patients in the intensive care unit. *CPT Pharmacometrics Syst Pharmacol.* 2024;13(5):823–36. <https://doi.org/10.1002/psp4.13121>.
 17. Yang Y, Xia Z, Xu C, Zhai C, Yu X, Li S. Ciprofol attenuates the isoproterenol-induced oxidative damage, inflammatory response and cardiomyocyte apoptosis. *Front Pharmacol.* 2022;13:1037151. <https://doi.org/10.3389/fphar.2022.1037151>.
 18. Dixon SJ, Lemberg KM, Lamprecht MR, Skouta R, Zaitsev EM, Gleason CE, Patel DN, Bauer AJ, Cantley AM, Yang WS, Morrison B 3rd, Stockwell BR. Ferroptosis: an iron-dependent form of nonapoptotic cell death. *Cell.* 2012;149(5):1060–72. <https://doi.org/10.1016/j.cell.2012.03.042>.
 19. Hassannia B, Vandenabeele P, Vanden Berghe T. Targeting ferroptosis to Iron Out Cancer. *Cancer Cell.* 2019;35(6):830–49. <https://doi.org/10.1016/j.ccell.2019.04.002>.
 20. Van Coillie S, Van San E, Goetschalckx I, Wiernicki B, Mukhopadhyay B, Tonnus W, Choi SM, Roelandt R, Dumitrascu C, Lamberts L, Dams G, Weyts W, Huysentruyt J, Hassannia B, Ingold I, Lele S, Meyer E, Berg M, Seurinck R, Saeyns Y, Vermeulen A, van Nuijs ALN, Conrad M, Linkermann A, Rajapurkar M, Vandenabeele P, Hoste E, Augustyns K, Vanden Berghe T. Targeting ferroptosis protects against experimental (multi)organ dysfunction and death. *Nat Commun.* 2022;13(1):1046. <https://doi.org/10.1038/s41467-022-28718-6>.
 21. Gupta U, Ghosh S, Wallace CT, Shang P, Xin Y, Nair AP, Yazdankhah M, Strizhakova A, Ross MA, Liu H, Hose S, Stepicheva NA, Chowdhury O, Nemani M, Maddipatla V, Grebe R, Das M, Lathrop KL, Sahel JA, Zigler JS Jr, Qian J, Ghosh A, Sergeev Y, Handa JT, St Croix CM, Sinha D. Increased LCN2 (lipocalin 2) in the RPE decreases autophagy and activates inflammasome-ferroptosis processes in a mouse model of dry AMD. *Autophagy.* 2023;19(1):92–111. <https://doi.org/10.1080/15548627.2022.2062887>.
 22. Liu P, Feng Y, Li H, Chen X, Wang G, Xu S, Li Y, Zhao L. Ferrostatin-1 alleviates lipopolysaccharide-induced acute lung injury via inhibiting ferroptosis. *Cell Mol Biol Lett.* 2020;25:10. <https://doi.org/10.1186/s11658-020-00205-0>.
 23. Liu C, Zou Q, Tang H, Liu J, Zhang S, Fan C, Zhang J, Liu R, Liu Y, Liu R, Zhao Y, Wu Q, Qi Z, Shen Y. Melanin nanoparticles alleviate sepsis-induced myocardial injury by suppressing ferroptosis and inflammation. *Bioact Mater.* 2022;24:313–21. <https://doi.org/10.1016/j.bioactmat.2022.12.026>.
 24. Habib E, Linher-Melville K, Lin HX, Singh G. Expression of xCT and activity of system xc(-) are regulated by NRF2 in human breast cancer cells in response to oxidative stress. *Redox Biol.* 2015;5:33–42. <https://doi.org/10.1016/j.redox.2015.03.003>.
 25. Ma CS, Lv QM, Zhang KR, Tang YB, Zhang YF, Shen Y, Lei HM, Zhu L. NRF2-GPX4/SOD2 axis imparts resistance to EGFR-tyrosine kinase inhibitors in non-small-cell lung cancer cells. *Acta Pharmacol Sin.* 2021;42(4):613–23. <https://doi.org/10.1038/s41401-020-0443-1>.
 26. Lu Z, Liu Z, Fang B. Propofol protects cardiomyocytes from doxorubicin-induced toxic injury by activating the nuclear factor erythroid 2-related factor 2/glutathione peroxidase 4 signaling pathways. *Bioengineered.* 2022;13(4):9145–55. <https://doi.org/10.1080/21655979.2022.2036895>.
 27. Nair AB, Jacob S. A simple practice guide for dose conversion between animals and human. *J Basic Clin Pharm.* 2016;7(2):27–31. <https://doi.org/10.4103/0976-0105.177703>.
 28. Hughes KT, Beasley MB. Pulmonary manifestations of Acute Lung Injury: more than just diffuse alveolar damage. *Arch Pathol Lab Med.* 2017;141(7):916–22. <https://doi.org/10.5858/arpa.2016-0342-RA>.
 29. Park I, Kim M, Choe K, Song E, Seo H, Hwang Y, Ahn J, Lee SH, Lee JH, Jo YH, Kim K, Koh GY, Kim P. Neutrophils disturb pulmonary microcirculation in sepsis-induced acute lung injury. *Eur Respir J.* 2019;53(3):1800786. <https://doi.org/10.1183/13993003.00786-2018>.
 30. Li R, Li X, Zhao J, Meng F, Yao C, Bao E, Sun N, Chen X, Cheng W, Hua H, Li X, Wang B, Wang H, Pan X, You H, Yang J, Ikezoe T. Mitochondrial STAT3 exacerbates LPS-induced sepsis by driving CPT1a-mediated fatty acid oxidation. *Theranostics.* 2022;12(2):976–98. <https://doi.org/10.7150/thno.63751>.
 31. Yuan D, Su G, Liu Y, Chi X, Feng J, Zhu Q, Cai J, Luo G, Hei Z. Propofol attenuated liver transplantation-induced acute lung injury via connexin43 gap junction inhibition. *J Transl Med.* 2016;14(1):194. <https://doi.org/10.1186/s12967-016-0954-1>.
 32. Becher T, Meiser A, Guenther U, Bellgardt M, Wallenborn J, Kogelmann K, Bracht H, Falthausen A, Nilsson J, Sackey P, Kellner P. Isoflurane vs. propofol for sedation in invasively ventilated patients with acute hypoxemic respiratory failure: an a priori hypothesis substudy of a randomized controlled trial. *Ann Intensive Care.* 2022;12(1):116. <https://doi.org/10.1186/s13613-022-01090-w>.
 33. Wang L, Tang X, Li S. Propofol promotes migration, alleviates inflammation, and apoptosis of lipopolysaccharide-induced human pulmonary microvascular endothelial cells by activating PI3K/AKT signaling pathway via upregulating APOM expression. *Drug Dev Res.* 2022;83(2):397–406. <https://doi.org/10.1002/ddr.21869>.
 34. Wu B, Zhu W, Wang Q, Ren C, Wang L, Xie G. Efficacy and safety of ciprofol-remifentanyl versus propofol-remifentanyl during fiberoptic bronchoscopy: a prospective, randomized, double-blind, non-inferiority trial. *Front Pharmacol.* 2022;13:1091579. <https://doi.org/10.3389/fphar.2022.1091579>.
 35. Liang P, Dai M, Wang X, Wang D, Yang M, Lin X, Zou X, Jiang K, Li Y, Wang L, Shangguang W, Ren J, He H. Efficacy and safety of ciprofol vs. propofol for the induction and maintenance of general anaesthesia: a multicentre, single-blind, randomised, parallel-group, phase 3 clinical trial. *Eur J Anaesthesiol.* 2023;40(6):399–406. <https://doi.org/10.1097/EJA.0000000000001799>.
 36. Liu X, Ren M, Zhang A, Huang C, Wang J. Nrf2 attenuates oxidative stress to mediate the protective effect of ciprofol against cerebral ischemia-reperfusion injury. *Funct Integr Genomics.* 2023;23(4):345. <https://doi.org/10.1007/s10142-023-01273-z>.
 37. Li J, Lu K, Sun F, Tan S, Zhang X, Sheng W, Hao W, Liu M, Lv W, Han W. Panaxydol attenuates ferroptosis against LPS-induced acute lung injury in mice by Keap1-Nrf2/HO-1 pathway. *J Transl Med.* 2021;19(1):96. <https://doi.org/10.1186/s12967-021-02745-1>.
 38. Shen K, Wang X, Wang Y, Jia Y, Zhang Y, Wang K, Luo L, Cai W, Li J, Li S, Du Y, Zhang L, Zhang H, Chen Y, Xu C, Zhang J, Wang R, Yang X, Wang Y, Hu D. miR-125b-5p in adipose derived stem cells exosome alleviates pulmonary microvascular endothelial cells ferroptosis via Keap1/Nrf2/GPX4 in sepsis lung injury. *Redox Biol.* 2023;62:102655. <https://doi.org/10.1016/j.redox.2023.102655>.
 39. Wang Y, Chen D, Xie H, Jia M, Sun X, Peng F, Guo F, Tang D. AUF1 protects against ferroptosis to alleviate sepsis-induced acute lung injury by regulating NRF2 and ATF3. *Cell Mol Life Sci.* 2022;79(5):228. <https://doi.org/10.1007/s00018-022-04248-8>.
 40. Yang WS, SriRamaratnam R, Welsch ME, Shimada K, Skouta R, Viswanathan VS, Cheah JH, Clemons PA, Shamji AF, Clish CB, Brown LM, Girotti AW, Cornish VW, Schreiber SL, Stockwell BR. Regulation of ferroptotic cancer cell death by GPX4. *Cell.* 2014;156(1–2):317–31. <https://doi.org/10.1016/j.cell.2013.12.010>.
 41. Koppula P, Zhuang L, Gan B. Cystine transporter SLC7A11/xCT in cancer: ferroptosis, nutrient dependency, and cancer therapy. *Protein Cell.* 2021;12(8):599–620. <https://doi.org/10.1007/s13238-020-00789-5>.
 42. Dodson M, Castro-Portuguez R, Zhang DD. NRF2 plays a critical role in mitigating lipid peroxidation and ferroptosis. *Redox Biol.* 2019;23:101107. <https://doi.org/10.1016/j.redox.2019.101107>.
 43. Wang Y, Yan S, Liu X, Deng F, Wang P, Yang L, Hu L, Huang K, He J. PRMT4 promotes ferroptosis to aggravate doxorubicin-induced cardiomyopathy via inhibition of the Nrf2/GPX4 pathway. *Cell Death Differ.* 2022;29(10):1982–95. <https://doi.org/10.1038/s41418-022-00990-5>.

Publisher's note

Springer Nature remains neutral with regard to jurisdictional claims in published maps and institutional affiliations.